ADVANCED FUNCTIONAL MATERIALS
www.afm-journal.de

Homogenizing the Electron Extraction via Eliminating Low-Conductive Contacts Enables Efficient Perovskite Solar Cells with Reduced Up-Scaling Losses

Zhineng Lan, Hao Huang, Yi Lu, Shujie Qu, Min Wang, Shuxian Du, Yingying Yang, Changxu Sun, Qiang Zhang, Yi Suo, Xinxin Wang, Luyao Yan, Peng Cui, Zhiguo Zhao, and Meicheng Li**

Maintaining the power conversion efficiency (PCE) of perovskite solar cells (PSCs) while enlarging the active area is necessary for their industrialization, where the key part is the uniform carrier extraction. Here, a conformal electron transport layer (ETL) is reported with eliminated low-conductive contacts through a tailored deposition that combines chemical bath deposition and modified spin-coating on a light-managing textured substrate. The KPFM and C-AFM are utilized to prove the uniform and optimized electrical properties. This study further employs the 2D measurements of PL and TRPL mapping to focus on revealing the enhanced uniformity of electron extraction. The uniform ETL conductivity and electron extraction contribute to a substantial decrease in device up-scaling losses, making the δ_{PCE} ($\frac{PCE_{0.08}-PCE_1}{PCE_{0.08}}$) between 0.08 cm^2-device and 1 cm^2-device decrease from 5.02% to 2.97%, while the perovskite film is deposited using two-step method. When using one-step method to deposit perovskite film, PCEs of 25.13% and 23.93% for the active area of 0.08 cm^2 and 1 cm^2 are achieved, and the δ_{PCE} decreases from 7.89% to 4.77%, validating the significant effects on reducing up-scaling losses. This work provides a new perspective to maintain high efficiency while device up-scaling, providing more opportunities to push forward the PSCs industrialization.

1. Introduction

Metal halide perovskite solar cells (PSCs) have been considered to be the most potential photovoltaic technology, due to its remarkable advantages like low-cost solution preparation, high efficiency, flexible and semi-transparent preparation, and so on.[1–6] Although significant improvements have been achieved in both power conversion efficiency (PCE) and stability, a challenge limiting their industrialization is the trade-off between the high efficiency and large active area, an issue determined not only by perovskite film but also the carrier transport layer.[7–12] Currently, massive literature related to perovskite regulation has been reported to enhance the photovoltaic performance of PSCs with an active area >1 cm^2.[13–17] Besides, as the research progresses, it is observed that the fill factor (FF) of the PSCs obviously declines as the active area increases. The declined FF is supposed to closely relate to the non-uniform interfacial electron extraction, an issue mainly determined by the electron transport layer (ETL), especially in planar n-i-p PSCs.[18–20] Proposing a tailored deposition to achieve a high-quality ETL with uniform electrical properties at the lateral aspect is expected to enhance the uniform electron extraction, leading to a decrease in the up-scaling loss of PSCs.

In planar PSCs, the fluorine-doped tin oxide (FTO) is the most popular substrate, its textured surface as the front contact that scatters the incoming radiation can destroy the coherence of the incoming light and afford light trapping by increasing the optical path length.[21,22] The enhanced light absorption is beneficial to the improvement of the short-circuit current density (J_{SC}) of PSCs. This similar strategy that uses the textured surface to enhance light absorption has been utilized in traditional silicon solar cells and emerging silicon/perovskite tandem solar cells.[23,24] Although the textured surface of FTO exhibits a positive effect on the J_{SC}, it is a challenge for the deposition of thin and uniform ETL.[25] Such a challenge is much more severe when the PSCs up-scaling to a large-area device. Therefore, it is necessary to develop a deposition strategy to obtain a conformal ETL on the textured substrate for efficient and scalable planar PSCs.

Z. Lan, H. Huang, Y. Lu, S. Qu, M. Wang, S. Du, Y. Yang, C. Sun, Q. Zhang, Y. Suo, X. Wang, L. Yan, P. Cui, M. Li
State Key Laboratory of Alternate Electrical Power System with Renewable Energy Sources
North China Electric Power University
Beijing 102206, China
E-mail: mcli@ncepu.edu.cn
Z. Zhao
Huaneng Clean Energy Research Institute
Beijing 100000, China
E-mail: zhao_zg@qny.chng.com.cn

The ORCID identification number(s) for the author(s) of this article can be found under https://doi.org/10.1002/adfm.202316591

DOI: 10.1002/adfm.202316591

To obtain high-quality ETL, several techniques, such as spin-coating, atom layer deposition, magnetron sputtering, and chemical bath deposition have been proposed.[26–28] Among them, spin-coating has been proven to be an available method to deposit high-quality ETL. However, this method is prone to produce a non-uniform film on the light-managing textured substrate, which is more suitable to be applied on a substrate like indium-doped tin oxide that exhibits a smooth surface.[29] Chemical bath deposition enables uniform and complete coverage on the underlying substrate, which is more suitable for depositing ETL on FTO substrate.[30,31] Recently, Yoo et al. achieved high-quality SnO_2 on FTO via chemical bath deposition by finely controlling the deposition process, resulting in a certified PCE of 25.2%.[32] However, the chemical reaction during the SnO_2 chemical bath deposition is complex and the property of deposited SnO_2 is particularly sensitive to the condition, which makes the technology of SnO_2 chemical bath deposition hard to be repeated. In comparison, the chemical bath deposition of TiO_2 has been extensively investigated and well-established much earlier, representing a mature technology with excellent reproducibility.[33] In 2022, Huang et al. proposed a ligand-engineered deposition strategy to precisely regulate the TiO_2 chemical bath deposition process, and simultaneously optimize the TiO_2 and its interfacial contact property, achieving a PCE of 24.8% with FF exceeding 83.1%.[25] Although the TiO_2 chemical bath deposition has been broadly used to deposit high-quality TiO_2 on FTO, the relatively low electron mobility ($\approx 10^{-5}$ cm^2 V^{-1} s^{-1}) and easily generated structural defects limit the efficient and uniform interfacial electron extraction, especially when applied to large-area devices. Hence, combining the advantage of different deposition methods and different ETL materials should be a feasible approach to fabricating ETL with excellent and uniform electronic properties on texture FTO for efficient PSCs.[34–36]

Here, we proposed a tailored deposition by combining the chemical bath deposition and spin-coating to achieve a conformal ETL of TiO_2/SnO_2 on texture FTO substrate. Furthermore, the deposition of the SnO_2 capping layer is further modified by the ammonium hypophosphite (AH), which homogenizes the SnO_2 distribution. The conformal ETL with eliminated low-conductive contacts enhanced the uniformity of electronic conductivity and interfacial electron extraction. The resulting PSCs where the perovskite films are fabricated by one-step method achieve PCEs of 25.13% and 23.93% for the active area of 0.08 and 1 cm^2, respectively, and the δ_{PCE} ($\frac{PCE_{0.08}-PCE_1}{PCE_{0.08}}$) between 0.08 cm^2-device and 1 cm^2-device decrease from 7.89% to 4.77%. The PSCs where the perovskite films are fabricated by two-step method achieve a small δ_{PCE} of 2.97%, validating the significant effects on reducing the up-scaling losses. This work can provide a technical reference for preparing the ETL on a textured substrate and a new insight into the reduction of up-scaling losses of PSCs.

2. Results and Discussion

2.1. The Fabrication and Characterization of ETLs

Considering the textured surface of FTO, we first deposited a TiO_2 layer by utilizing the chemical bath method, because this method can ensure a conformal and uniform deposition. Then, to optimize and homogenize the electronic property and alleviate the diverse impact of the TiO_2 on perovskite, we deposited a SnO_2 capping layer on the surface of TiO_2. When depositing the SnO_2 capping layer, the AH (the molecular structure shown in Figure S1, Supporting Information) was incorporated to assist the deposition by enhancing the adhesion of SnO_2 on TiO_2, which is explained and supported by Figures S2 and S3 (Supporting Information). Notably, the SnO_2 with AH is named as AH-SnO_2. For characterizing the morphology of different ETLs, we prepared TiO_2, TiO_2/SnO_2, and TiO_2/AH-SnO_2, respectively (**Figure 1a**). The scanning electron microscope (SEM) measurement was performed to observe the surface morphology of ETLs with the results shown in Figure 1b-d. We can clearly observe the compact and continuous TiO_2 film on FTO. The topography of FTO is obviously observed, which indicates that TiO_2 film is deposited conformably. The cross-sectional SEM image exhibited in the inset also validates the conformal deposition of TiO_2. In addition, there are many coral-like clusters and protrusions located on the surface of TiO_2, which may result from the violent hydrolysis reaction and active intermediate products during the chemical bath process. This phenomenon has also been observed and reported in our previous work.[25] After depositing TiO_2 film on the textured FTO, the SnO_2 capping layer was deposited by spin-coating method. From the surface and cross-sectional SEM image, the SnO_2 capping layer has negligible influence on the overall surface morphology of TiO_2. However, in detail, we can find that the coral-like clusters are mitigated, such a phenomenon is also observed in TiO_2/AH-SnO_2 after incorporating the AH into the SnO_2 capping layer. The mitigated clusters may come from the SnO_2 wrapping, which softens the outline of the nanocluster and destroys the weak nanostructure.[37–39]

To quantify the surface differences of TiO_2, TiO_2/SnO_2, and TiO_2/AH-SnO_2, atomic force microscopy (AFM) was used to further characterize surface morphology and roughness. As shown in Figure S4 (Supporting Information), the AFM images remain consistent with the above SEM images, where we can clearly observe the FTO topography, demonstrating the conformal deposition of ETLs. The clusters and protrusions can also be observed, which is supposed to influence the surface roughness. The root mean square (RMS) of TiO_2, TiO_2/SnO_2, and TiO_2/AH-SnO_2 is 17, 16, and 14 nm, respectively. The RMS is reduced after depositing the SnO_2 capping layer and further AH incorporation, which validates the mitigation of surface clusters. The results of SEM and AFM prove that the tailored deposition including chemical bath and spin-coating can ensure a conformal ETL on the textured FTO, and the SnO_2 capping layer and further AH incorporation possess a positive effect on reducing the surface roughness and increasing the surface uniformity.

Except for the surface morphology, we characterize properties of ETLs such as surface potential, conductivity, and energy levels. First, X-ray photoelectron spectroscopy (XPS) was carried out to confirm the successful deposition of the SnO_2 capping layer. As shown in Figure 1e and Figure S5 (Supporting Information), compared to the XPS spectrum of TiO_2, there is an obvious peak of Sn 3d and Sn 4s in the spectrum of TiO_2/SnO_2, demonstrating that SnO_2 is spin-coated on TiO_2. As for the TiO_2/AH-SnO_2, it is observed a new peak located at 133.20 eV that denotes the hypophosphite group of AH in the P 2p spectrum (Figure 1e), confirming the incorporation of AH in AH-SnO_2.[9]

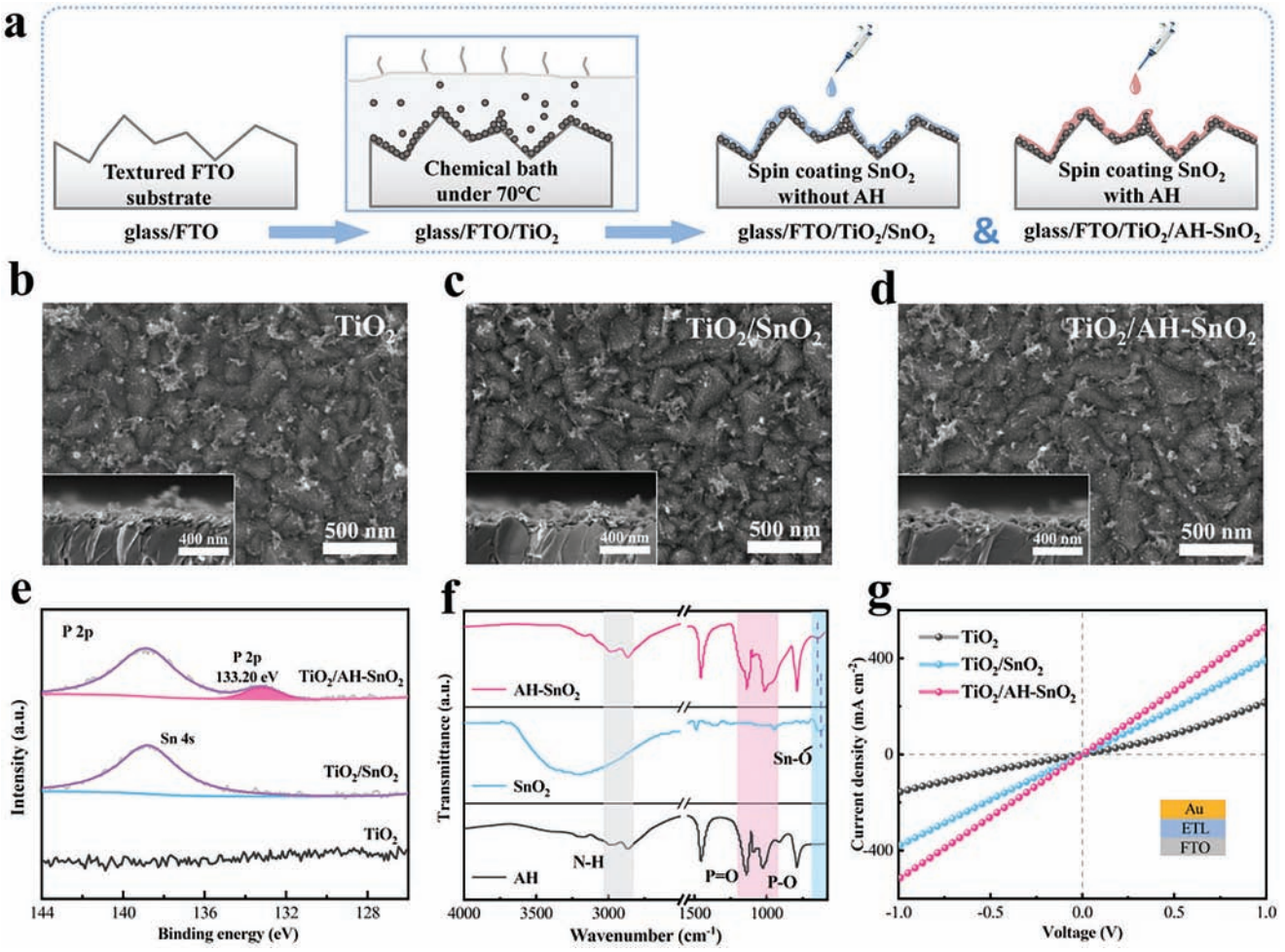

Figure 1. The preparation process and morphology of ETLs. a) The schematic diagram of the preparation process of ETLs. b–d) Surface SEM images of ETLs, the corresponding cross-sectional SEM image is illustrated as inset. e) XPS spectra of P 2p for ETL_S. f) FTIR spectra of AH, SnO_2, and AH-SnO_2, all the sample is powder, and the SnO_2 and AH-SnO_2 powder are obtained by drying the corresponding solution. g) *J–V* curves of devices including different ETLs under dark.

Meanwhile, the peak shift of Sn $3d_{3/2}$ and Sn $3d_{5/2}$ is observed in the high-resolution Sn 3d spectrum in TiO_2/AH-SnO_2 compared to that of TiO_2/SnO_2 (Figure S6, Supporting Information), indicating the chemical interaction between AH and Sn atom. The successful incorporation of AH in SnO_2 was also validated by Fourier transform infrared spectrometer (FTIR) measurement (Figure 1f; Figure S7, Supporting Information). The SnO_2 capping layer and its modification by incorporating AH possess a positive effect on the conductivity of ETL. We compared the conductivity among these ETLs by fabricating devices structured as FTO/ETLs/Au. Figure 1g shows that the conductivity of TiO_2/SnO_2 is higher than that of TiO_2, which agrees with the previous reports.[26,40] Moreover, the conductivity of TiO_2/SnO_2 has further been increased with the incorporation of AH, which can be attributed to the enhanced contact between SnO_2 and TiO_2.

The energy level structure of ETLs was also characterized by Kelvin probe force microscopy (KPFM) and ultraviolet photoelectron spectroscopy (UPS). First, The KPFM was performed to characterize the surface potential of these ETLs (**Figure** 2a-c). The distribution of surface potential and average value have been exhibited. The average surface potential of TiO_2/AH-SnO_2 (9 mV) is lower than that of TiO_2 (61 mV) and TiO_2/SnO_2 (33 mV), indicating an upshift of the Fermi level (E_F). The corresponding RMS values of TiO_2, TiO_2/SnO_2, and TiO_2/AH-SnO_2 are 3.9, 2.3, and 1.9 mV, respectively. The reduced RMS indicates that the uniformity of surface potential is enhanced. The detailed energy level structure was determined by UPS (Figure S8, Supporting Information). The E_F of TiO_2/AH-SnO_2 film (−4.01 eV) is higher than that of TiO_2/SnO_2 (−4.09 eV) and TiO_2 (−4.48 eV), which is consistent with the KPFM results. Besides, combining the Fermi edges, we further calculate the valence band maximum energy (E_{VBM}) of TiO_2 to be −7.51 eV, and the E_{VBM} of SnO_2 to be −8.11 eV, and the E_{VBM} of AH-SnO_2 to be −7.96 eV. The band gap values of TiO_2, SnO_2, and AH-SnO_2 can be obtained through tauc plots (Figure S9, Supporting Information). Based on the results of USP and tauc plots, the conduction band minimum energy (E_{CBM}) is calculated to be −4.36, −3.79, and −3.61 eV for TiO_2, SnO_2, and AH-SnO_2, respectively. The optimized energy level and constructed gradient level structure are supposed to enhance the interfacial electron extraction,

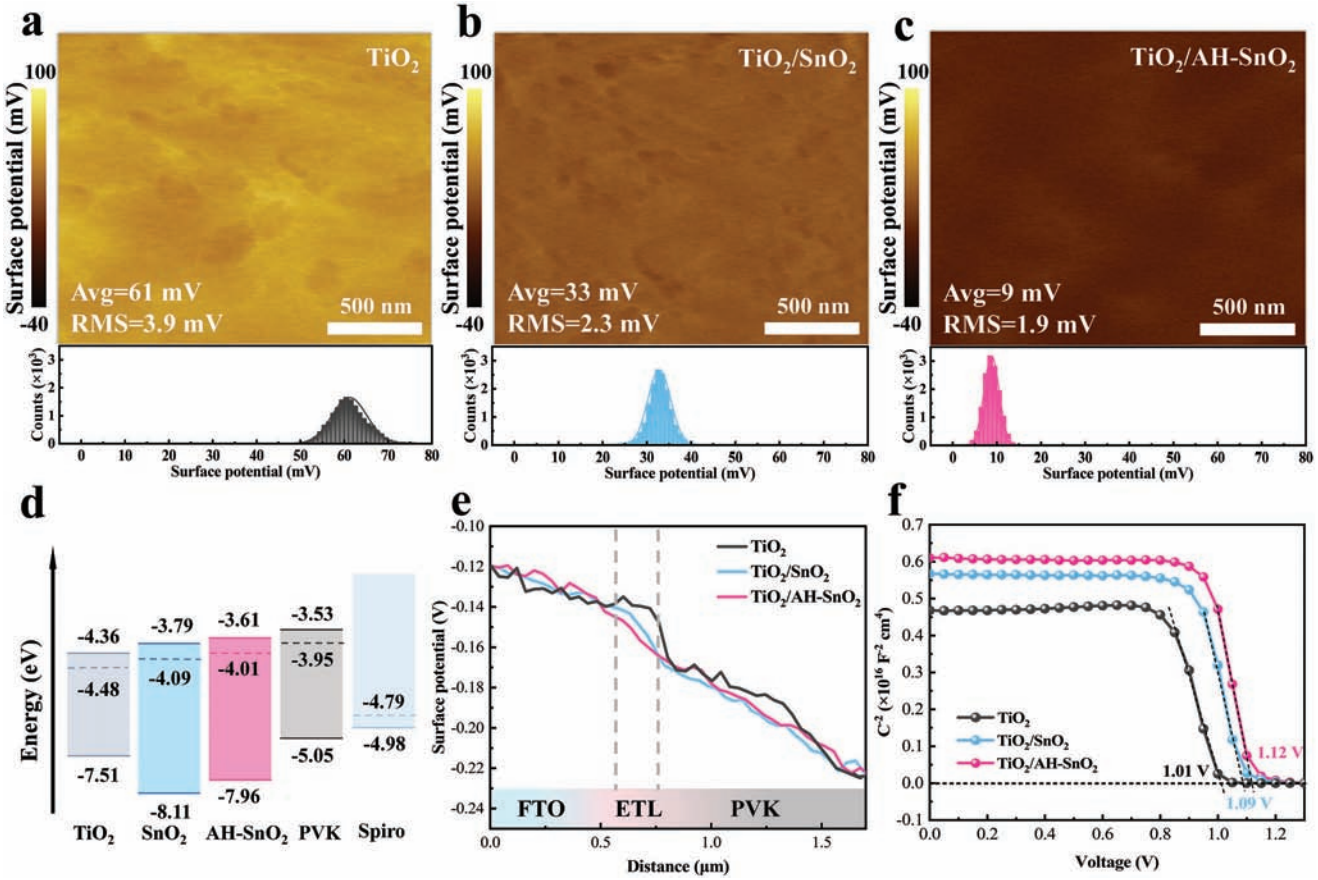

Figure 2. Characterization of ETLs. a–c) KPFM images and corresponding surface potential distribution of ETLs. d) Schematic diagram of the energy level structure. e) The surface potential curve of FTO/ETLs/perovskite cross-section. f) Mott–Schottky plots of PSCs with different ETL under dark conditions.

contributing to the photovoltaic performance improvement of PSCs (Figure 2d; Figures S10 and S11, Supporting Information). We proposed a schematic diagram of the band bending shown in Figure S12 (Supporting Information). The energy level offset ($\Delta E = E_{CBM\ (Perovskite)} - E_{CBM\ (ETLs)}$) can be effectively reduced by introducing a capping layer. We also characterized the cross-sectional KPFM image of FTO/ETLs/perovskite to directly show the interfacial potential changes.[41] As shown in Figure 2e and Figure S13 (Supporting Information), The potential slope can be mitigated by SnO_2 and AH-SnO_2, indicating that the capping layer can effectively optimize the interface energy level matching, which is consistent with the UPS results. We measured Mott–Schottky plots of PSCs with different ETLs to evaluate the interface and charge transport properties with the results shown in Figure 2f. It can be seen that the PSCs based on TiO_2, TiO_2/SnO_2, and TiO_2/AH-SnO_2 show a built-in field (V_{bi}) of 1.01, 1.09, and 1.12 V, respectively. The higher V_{bi} mainly resulted from the optimized interfacial energy level matching is beneficial for the separation of photogenerated electron–hole pairs and further promotes carrier transport. We preliminary fabricated planar PSCs with different ETLs and collects their photovoltaic parameters. Due to the poor carrier transport characteristics of TiO_2 ETL, TiO_2-based PSCs possess a less-than-ideal PCE (Figure S14 and Table S1, Supporting Information).

2.2. The Enhanced Electron Extraction and Photovoltaic Performance of PSCs

The SnO_2 capping layer can effectively improve the PCE of TiO_2-based PSCs, which is consistent with the reported works.[42,43] Thereafter, we focus on the investigation of the AH-SnO_2 capping layer and its influence on the PSCs performance. To investigate the interfacial electron transport dynamic and the device physics, various measurements were performed on PSCs with TiO_2/SnO_2 and TiO_2/AH-SnO_2. The steady-state photoluminescence (PL) was carried out to investigate the influence of AH on interfacial electron transport (**Figure 3a**). Compared to the spectrum of perovskite film on TiO_2/SnO_2, the spectrum of perovskite film on TiO_2/AH-SnO_2 shows tremendous quenching of PL intensity, indicating more effective electron extraction. Based on the curve fitting of time-resolved photoluminescence (TRPL) spectra (Figure 3b), the average carrier lifetimes (τ_{avg}) can be calculated. The τ_{avg} of perovskite deposited on TiO_2/AH-SnO_2 is 616.53 ns, which is much lower than that (903.13 ns) of perovskite deposited on TiO_2/SnO_2. These results testify that TiO_2/AH-SnO_2 has an enhanced electron extraction ability. Furthermore, to gain an insight into the trap-assisted charge recombination in the device, the dependence of open-circuit voltage on the light intensity was investigated

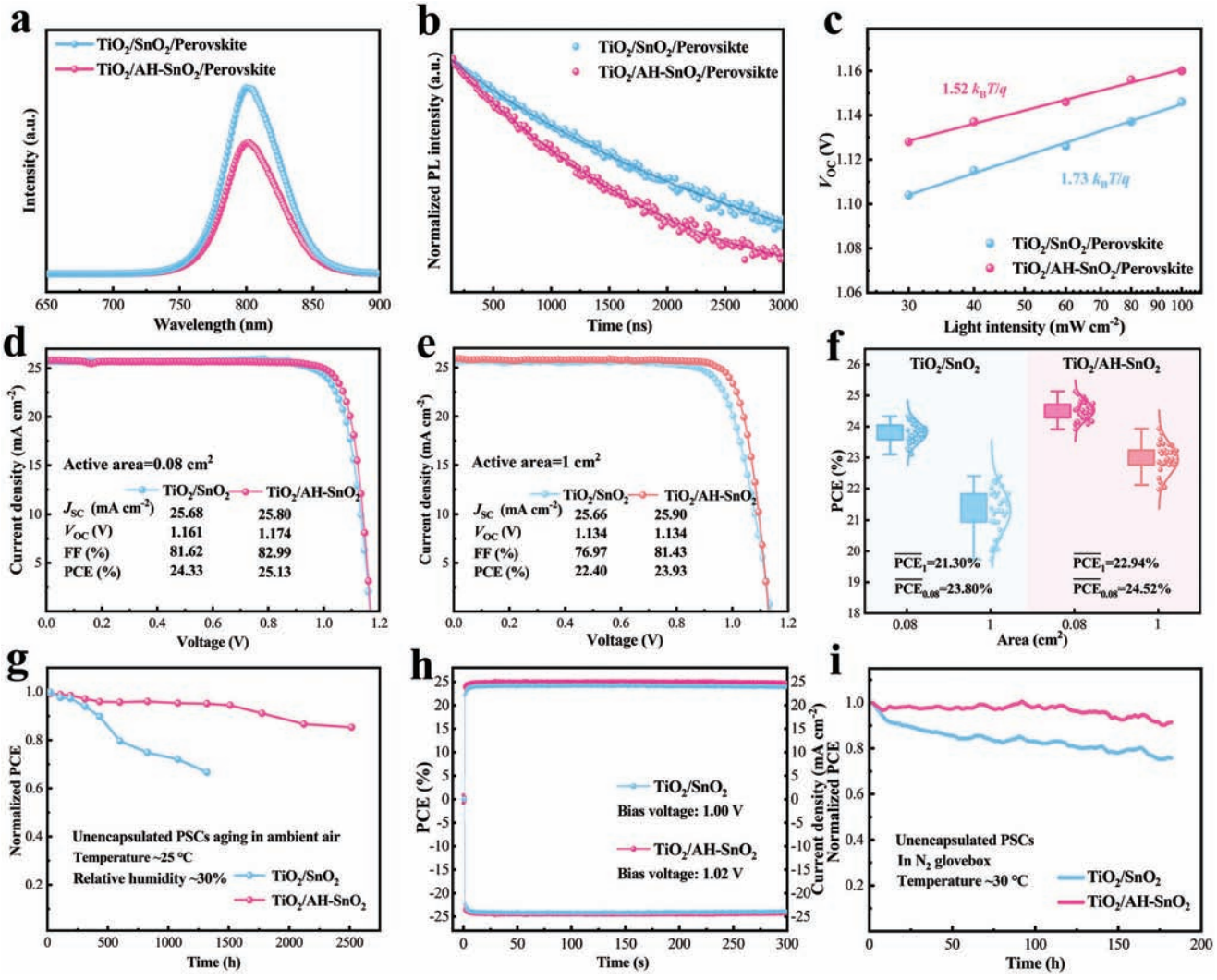

Figure 3. Performance of PSCs with different ETLs. a) PL spectra of perovskite films deposited on different ETLs. b) TRPL spectra of perovskite films deposited on different ETLs. c) V_{OC} of PSCs with various ETLs plotted against the logarithm of light intensity. d) Reverse *J–V* curves of champion PSCs with different ETLs, the active area is 0.08 cm^2. e) Reverse *J–V* curves of champion PSCs with different ETLs, the active area is 1 cm^2. f) Statistical results of PCEs, each group has 40 devices for 0.08 cm^2-PSCs, and each group has 35 devices for 1 cm^2-PSCs. g) The PCE evolution of unencapsulated PSCs with different ETLs aged in ambient air. h) Steady-state efficiency at the maximum power point for PSCs with different ETLs. i) Operational stability tracking of PSCs under steady-state light illumination and bias voltage for 180 h (N_2 atmosphere, white LED).

(Figure 3c). The ideal factor (n_{ID}) is obtained through the equation of $V_{OC} = nk_BTln(I)/q$, where k_B is the Boltzmann constant, T is the absolute temperature, and q is the electron charge.[44] The PSCs with TiO_2/AH-SnO_2 exhibit a smaller n_{ID}, suggesting that the non-radiative carrier recombination has been reduced, which is consistent with the dark current curves result (Figure S15 and Note S1, Supporting Information). The reduced non-radiative carrier recombination may result from enhanced interfacial electron extraction and passivated interface defects (Figures S16–S18 and Notes S2 and S3, Supporting Information).[45–47]

To explore the influence of the AH-SnO_2 capping layer on the PSCs photovoltaic performance, we fabricated PSCs with TiO_2/SnO_2 and TiO_2/AH-SnO_2 as ETL, where the perovskite film was deposited using the one-step method. Figure 3d displays the reverse *J–V* curves of the champion PSCs where the active area is 0.08 cm^2. The PSC with TiO_2/AH-SnO_2 obtained a PCE of 25.13%, with a V_{OC} of 1.174 V, a J_{SC} of 25.80 mA cm^{-2}, and an FF of 82.99%. In comparison, the PSC with TiO_2/SnO_2 obtains a lower PCE of 24.33%, with a V_{OC} of 1.161 V, a J_{SC} of 25.68 mA cm^{-2}, and an FF of 81.62% (Table S2, Supporting Information). The PSC with TiO_2/AH-SnO_2 also shows a reduced hysteresis, which should result from enhanced interfacial electron extraction and reduced interfacial carriers accumulation (Figure S19 and Table S2, Supporting Information).[48–50] The external quantum efficiency (EQE) spectra of corresponding PSCs are shown in Figure S20 (Supporting Information), where the integrated J_{SC} values possess a small variation from the values obtained from *J–V* curves. Besides, we also fabricated the PSCs with an active area of 1 cm^2 to investigate the

applicability of TiO_2/AH-SnO_2 on the scalable device. We are pleasantly surprised to find that the 1 cm^2-PSCs with TiO_2/AH-SnO_2 show a high PCE of 23.93% with a reduced hysteresis, while the 1 cm2-PSCs with TiO_2/SnO_2 only have a PCE of 22.40% (Figure 3e; Figure S21 and Table S3, Supporting Information). To verify the reproducibility, we further fabricated a batch of 0.08 cm^2-PSCs with TiO_2/SnO_2 and TiO_2/AH-SnO_2, respectively, and 40 devices were included in this batch. The statistics of photovoltaic parameters are shown in Figure 3f and Figure S22 (Supporting Information). Both the PSCs possess good reproducibility and the average PCE of PSCs with TiO_2/AH-SnO_2 is 24.52%, higher than that of 23.80% of PSCs with TiO_2/SnO_2. A batch of 1 cm^2-PSCs with different ETLs was also fabricated, each type of PSCs includes 35 devices (Figure 3f; Figure S23, Supporting Information). It is obvious that the 1 cm^2-PSCs with TiO_2/AH-SnO_2 not only exhibit an improved reproducibility but also an improved average PCE, compared to the 1 cm^2-PSCs with TiO_2/SnO_2. In detail, we can also find that the PCE increment after incorporating AH in the SnO_2 capping layer is much bigger in the 1 cm^2-PSCs compared to that in the 0.08 cm^2-PSCs. With the active area of PSCs changing from 0.08 to 1 cm^2, the average PCE of PSCs with TiO_2/SnO_2 decreases from 23.80% to 21.30%. As a comparison, the average PCE of PSCs with TiO_2/AH-SnO_2 decreases from 24.52% to 22.94%. The smaller PCE reduction demonstrates that the TiO_2/AH-SnO_2 exhibits huge potential for scalable manufacturing of efficient PSCs.

Besides the photovoltaic performance, the stability of PSCs is also characterized by continuous monitoring of the PCE evolution after long-term storage and output. For the stability measurement, the structure of PSCs is also FTO/TiO_2/SnO_2 (AH-SnO_2)/PVK/Spiro-OMeTAD/Au. The PCEs of unencapsulated PSCs with TiO_2/SnO_2 layer and TiO_2/AH-SnO_2 stored in ambient air with 25 °C and 30% relative humidity for 2500 h were monitored (Figure 3g). The PSCs with TiO_2/AH-SnO_2 layer can maintain 85% of their initial PCE after 2500 h, while PSCs with TiO_2/SnO_2 drop to 80% of its initial PCE after ≈500 h. The corresponding *J–V* curves are shown in Figure S24 (Supporting Information). Moreover, the stabilized PCE and its continuous evolution were also measured. Figure 3h shows the stabilized current density and PCE under one-sun illumination. The stabilized PCE of PSC with TiO_2/AH-SnO_2 is 24.88%, which is higher than that (23.89%) of PSCs with TiO_2/SnO_2. The results of operational stability are shown in Figure 3i, the PSCs with TiO_2/AH-SnO_2 can maintain ≈90% of the initial PCE after operating for 180 h, while the PSCs with TiO_2/AH-SnO_2 only maintained 70% of the initial value. The enhanced device stability can also be reflected from the enhanced interface stability through the measurements of EIS, open-circuit photovoltage decay, and transient ion-migration currents (Figures S25–S27, Tables S4 and S5, and Notes S4–S6, Supporting Information).[51,52] These results indicate that the of electron accumulation at the TiO_2/SnO_2/perovskite interface increases as the aging time prolongs, accompanied by the intensification of interfacial recombination and ion migration. As a comparison, these phenomena are effectively mitigated at TiO_2/AH-SnO_2/perovskite interface. The above results demonstrate that the modification of the SnO_2 capping layer can effectively improve the PSCs photovoltaic performance and also possess a positive effect on stability.

2.3. The Uniform Electron Extraction and Reduced Upscaling-Loss

TiO_2/AH-SnO_2 exhibits excellent application in large-area PSCs, which is supposed to be ascribed to its homogeneous electron extraction. To accurately characterize the electrical properties of TiO_2/SnO_2 and TiO_2/AH-SnO_2 in a wider landscape, we have carried out various characterization methods that can display 2D information. First, conducting atomic force microscope (C-AFM) was utilized to evaluate the surface conductivity and its distribution. As shown in **Figure** 4a,b, it is found that the average surface current of TiO_2/AH-SnO_2 is 716 pA, which is higher than that (660 pA) of TiO_2/SnO_2. The validated increased conductivity agrees with the results of *J–V* tests with the results in Figure 1g. We can further observe the surface current distribution from the C-AFM measurement (Figure 4c). The surface current of TiO_2/SnO_2 distributes within a range from 500 to 800 pA, and the corresponding RMS is 55 pA. As a comparison, the surface current of TiO_2/AH-SnO_2 distributes within a range from 600 to 800 pA, and the corresponding RMS is 30 pA. The increased average surface current and decreased RMS value demonstrate that the incorporation of AH eliminates low-conductive contacts and optimizes the uniformity of surface conductivity, which may result from the AH assisting the homogeneous deposition of SnO_2 capping layer.

The above results of PL and TRPL have proved that the TiO_2/AH-SnO_2 possesses a stronger electron extraction than TiO_2/SnO_2. Now, the PL and TRPL mapping were performed to focus on the lateral homogenous. From Figure 4d,e, we can find that the average PL intensity of perovskite on TiO_2/SnO_2 is lower than that of perovskite on TiO_2/AH-SnO_2, which verifies the enhanced electron extraction after the incorporation of AH. More importantly, the distribution of PL intensity has been effectively optimized. The PL intensity range of perovskite film on TiO_2/SnO_2 is from 250 to 1800, resulting in the mass of the local region with ultra-high intensity in the image (Figure 4f). As a comparison, the PL intensity range of perovskite film on TiO_2/AH-SnO_2 is from 250 to 800 with negligible high-intensity point distributing in a range from 1000 to 1200. The results of PL mapping demonstrated that the AH-SnO_2 capping layer effectively eliminates the local region with inefficient electron extraction, leading to a homogeneous interfacial electron transfer. The enhanced electron extraction of the AH-SnO_2 capping layer has also been proved by TRPL mapping measurement with the results shown in Figure 4g,h. From the lifetime distribution (Figure 4i), we can also find that the AH-SnO_2 capping obviously optimizes the uniformity of electron extraction, which is consistent with the results of PL mapping.

The schematic diagram was proposed to directly show the comparison of lateral uniform electron extraction and non-uniform electron extraction, which is demonstrated by PL mapping and TRPL mapping. As shown in **Figure** 5a, the AH-SnO_2 capping layer effectively decreases the local region of inefficient electron extraction, because the AH assists the deposition of SnO_2 on TiO_2, even in the TiO_2 cluster, which reduces the low-conductive location. The uniform deposition of the AH-SnO_2 capping layer reduces the variance of electrical properties at the lateral aspect, leading to uniform electron extraction. When the active area of PSCs is enlarged, this uniform electron

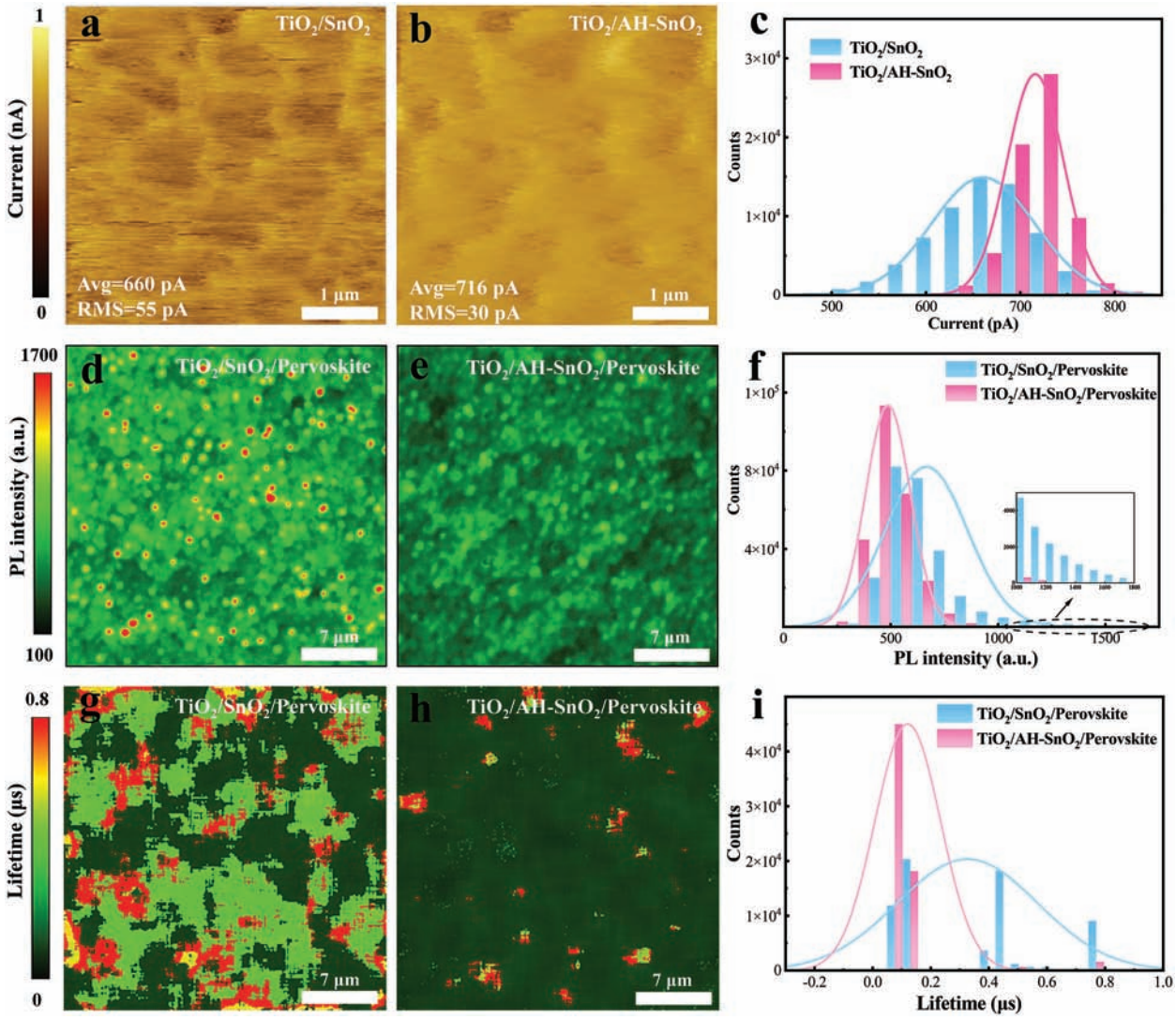

Figure 4. Uniform electron extraction. a,b) C-AFM images of ETLs. c) The corresponding surface current distribution of ETLs. d,e) PL mapping of perovskite films deposited on different ETLs. f) The corresponding PL intensity distribution. g,h) TRPL mapping of perovskite films deposited on different ETLs. i) The corresponding lifetime distribution.

extraction can be beneficial to reduce the efficiency decrease, which is proved by the PCE comparison of 0.08 cm^2-PSCs and 1 cm^2-PSCs in the above discussion. To further validate this point, we utilize a different method, two-step method, to deposit perovskite film on TiO_2/AH-SnO_2 and TiO_2/AH-SnO_2, respectively. Notably, in the later part of this paragraph, the PSCs are based on perovskite thin films prepared by a two-step method unless otherwise specified.

The PCE of champion 0.08 cm^2-PSC with TiO_2/AH-SnO_2 is 24.57%, which is higher than that (23.85%) of PSC with TiO_2/SnO_2 (Figure 5b; Figure S28 and Table S6, Supporting Information). As for the large-area devices, the 1 cm^2-PSCs with TiO_2/AH-SnO_2 obtain a PCE of 23.84%, J_{SC} is 25.89 mA cm^{-2}, V_{OC} is 1.147 V and FF is 80.27%. In contrast, the 1 cm^2-PSC with TiO_2/SnO_2 only obtain a PCE of 22.33%, J_{SC} is 25.83 mA cm^{-2}, V_{OC} is 1.121 V and FF is 77.08% (Figure 5c; Figure S29 and Table S7, Supporting Information). The reproducibility of both PSCs with different areas was characterized by fabricating a batch of devices and collecting their photovoltaic parameters. As shown in Figure 5d and Figures S30 and S31 (Supporting Information), all the PSCs possess good reproducibility and we can also find that the average PCE has been effectively improved after modifying the SnO_2 capping layer.

We use δ_{PCE} which can be calculated from the equation of $\frac{PCE_{0.08}-PCE_1}{PCE_{0.08}}$ to define the efficiency loss when the active area is enlarged from 0.08 to 1 cm^2. As shown in Figure 5e, when preparing the perovskite film using one-step method, the δ_{PCE} is 7.89% for the PSCs with TiO_2/SnO_2, and the δ_{PCE} is 4.77% for the PSCs with TiO_2/AH-SnO_2. When preparing the perovskite film using two-step method, for PSCs with TiO_2/SnO_2, the δ_{PCE} is 5.02%. As a comparison, the δ_{PCE} of PSCs with TiO_2/AH-SnO_2 is 2.97%, which is one of the minimum values among the previous works

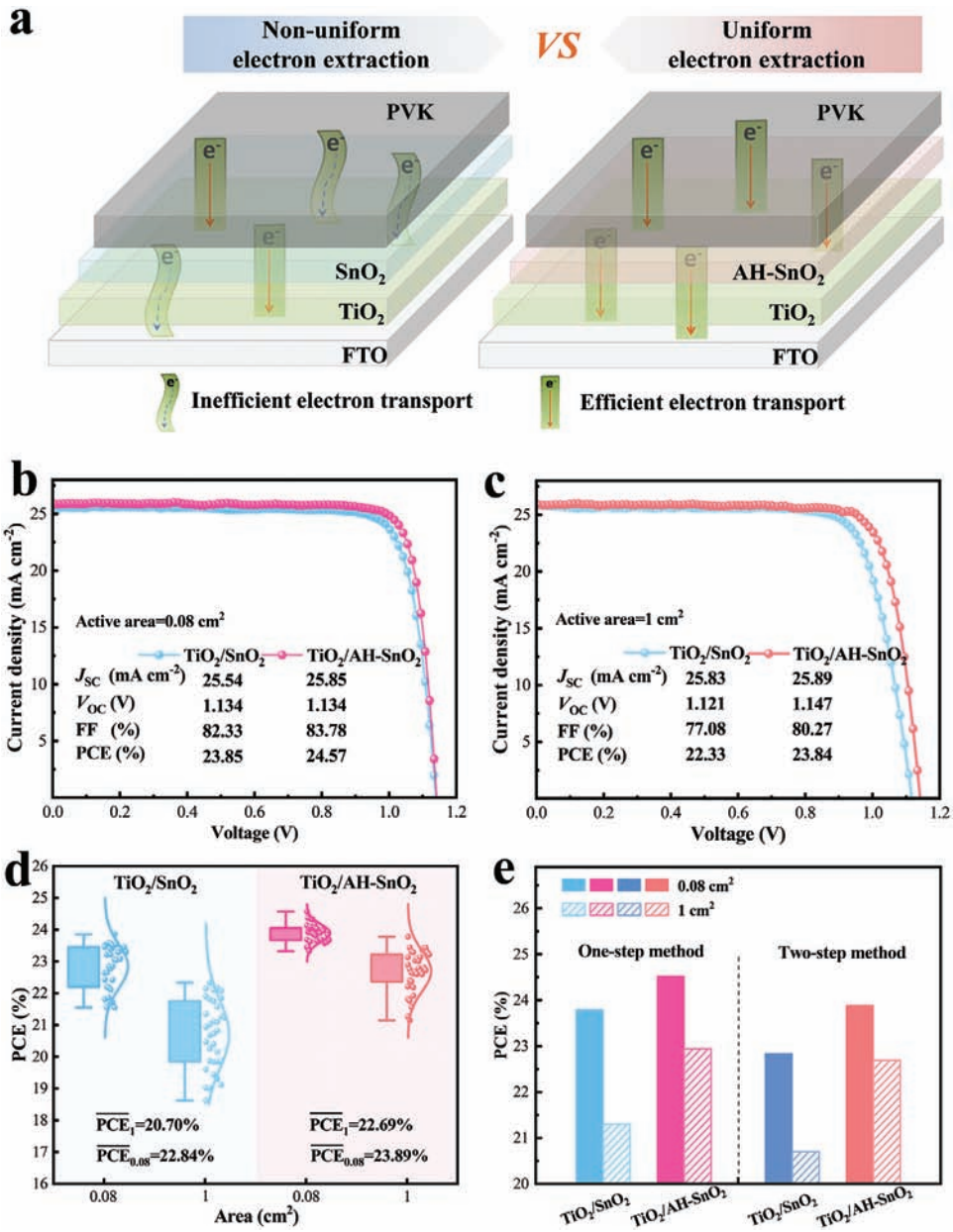

Figure 5. Application of ETLs on scalable PSCs where the perovskite film is prepared by two-step method. a) Schematic diagram of lateral uniform electron extraction. b) Reverse *J–V* curves of the champion PSCs, the active area is 0.08 cm^2. c) Reverse *J–V* curves of the champion PSCs, the active area is 1 cm^2. d) Statistical results of PCEs, each group has 40 devices for 0.08 cm^2-PSCs, and each group has 35 devices for 1 cm^2-PSCs. e) The average PCEs of PSCs, prepared by one-step and two-step with different active areas.

which reported the 0.08 cm^2-PSCs and 1 cm^2-PSCs (Figure S32 and Table S8, Supporting Information). Due to the enhanced uniformity of electron extraction, the novel ETL of TiO_2/AH-SnO_2 can effectively decrease the PCE loss during the device up-scaling, showing the great potential of promoting PSCs industrialization.

3. Conclusion

In this work, we have achieved high-efficiency PSCs with reduced up-scaling losses by depositing a conformal ETL on light-managing textured substrates. The tailored deposition combining chemical bath deposition and modified spin-coating eliminates the low-conductive contacts at ETL/perovskite interface, which improves the uniformity of electron extraction. We achieved a PCE of 25.13% for 0.08 cm^2-PSCs and 23.93% for 1 cm^2-PSCs, showing an effective reduction of the PCE loss between 0.08 cm^2-PSCs and 1 cm^2-PSCs with the δ_{PCE} decrease from 7.89% to 4.77%. Moreover, as for different perovskite films, the novel ETL of TiO_2/AH-SnO_2 also can effectively decrease the PCE loss with a small δ_{PCE} of 2.97%, which is one of the minimum values among the previous works, validating the significant

effects on reducing up-scaling losses. In addition, these resulting PSCs also possess excellent long-term storage stability and operating stability. This work provides more opportunities for the preparation of high-efficiency PSCs and a feasible approach for realizing their large-scale production with low energy loss.

4. Experimental Section

The experimental section/methods are shown in the Supporting Information.

Supporting Information

Supporting Information is available from the Wiley Online Library or from the author.

Acknowledgements

Z.L. and H.H. contributed equally to this work. This work is supported partially by the Key Research and Development Program sponsored by the Ministry of Science and Technology (MOST) (Grant nos. 2022YFB4200301), National Natural Science Foundation of China (Grant nos. 52232008, 51972110, 52102245, and 52072121), Beijing Natural Science Foundation (2222076, 2222077), Beijing Science and Technology Planning Project (Z211100004621010), Beijing Nova Program (20220484016), Young Elite Scientists Sponsorship Program by CAST (2022QNRC001), 2022 Strategic Research Key Project of Science and Technology Commission of the Ministry of Education, Huaneng Group Headquarters Science and Technology Project (HNKJ20-H88), the Fundamental Research Funds for the Central Universities (2022MS029, 2022MS02, 2022MS031, 2023MS042) and the NCEPU "Double First-Class" Program.

Conflict of Interest

The authors declare no conflict of interest.

Data Availability Statement

The data that support the findings of this study are available from the corresponding author upon reasonable request.

Keywords

electron extraction, electron transport layer, perovskite solar cells, SnO_2, TiO_2

Received: December 25, 2023
Revised: April 7, 2024
Published online:

[1] Best Research-Cell Efficiency Chart, https://www.nrel.gov/pv/cell-efficiency.html, (accessed:December 2023).
[2] P. Čulík, K. Brooks, C. Momblona, M. Adams, S. Kinge, F. Maréchal, P. J. Dyson, M. K. Nazeeruddin, *ACS Energy Lett.* **2022**, *7*, 3039.
[3] M. Jung, S. G. Ji, G. Kim, S. I. Seok, *Chem. Soc. Rev.* **2019**, *48*, 2011.
[4] P. Cui, D. Wei, J. Ji, H. Huang, E. Jia, S. Dou, T. Wang, W. Wang, M. Li, *Nat. Energy* **2019**, *4*, 150.
[5] T. Nie, Z. Fang, X. Ren, Y. Duan, S. Liu, *Nano-Micro Lett.* **2023**, *15*, 70.
[6] J. Liu, T. Ye, D. Yu, S. Liu, D. Yang, *Angew. Chem., Int. Ed.* **2023**, *62*, e202307225.
[7] Q. Jiang, R. Tirawat, R. A. Kerner, E. A. Gaulding, Y. Xian, X. Wang, J. M. Newkirk, Y. Yan, J. J. Berry, K. Zhu, *Nature* **2023**, *623*, 313.
[8] L. Yan, H. Huang, P. Cui, S. Du, Z. Lan, Y. Yang, S. Qu, X. Wang, Q. Zhang, B. Liu, X. Yue, X. Zhao, Y. Li, H. Li, J. Ji, M. Li, *Nat. Energy* **2023**, *8*, 1158.
[9] S. Yu, Z. Xiong, H. Zhou, Q. Zhang, Z. Wang, F. Ma, Z. Qu, Y. Zhao, X. Chu, X. Zhang, J. You, *Science* **2023**, *382*, 1399.
[10] J. Peng, F. Kremer, D. Walter, Y. Wu, Y. Ji, J. Xiang, W. Liu, T. Duong, H. Shen, T. Lu, F. Brink, D. Zhong, L. Li, O. Lee Cheong Lem, Y. Liu, K. J. Weber, T. P. White, K. R. Catchpole, *Nature* **2022**, *601*, 573.
[11] J. Zhou, H. Li, L. Tan, Y. Liu, J. Yang, R. Hua, C. Yi, *Angew. Chem., Int. Ed.* **2023**, *62*, e202300314.
[12] C. Fei, N. Li, M. Wang, X. Wang, H. Gu, B. Chen, Z. Zhang, Z. Ni, H. Jiao, W. Xu, Z. Shi, Y. Yan, J. Huang, *Science* **2023**, *380*, 823.
[13] K. l. Wang, M. Li, Y. H. Lou, J. Chen, Y. R. Shi, C. H. Chen, Y. H. Zhou, Z. K. Wang, L. S. Liao, *Adv. Energy Mater.* **2023**, *13*, 2203471.
[14] L. Xu, H. Ji, W. Qiu, X. Wang, Y. Liu, Y. Li, J. Li, X. Zhang, D. Zhang, J. Wang, Y. Tao, M. Li, R. Chen, *Adv. Mater.* **2023**, *35*, 2301752.
[15] H. Li, J. Zhou, L. Tan, M. Li, C. Jiang, S. Wang, X. Zhao, Y. Liu, Y. Zhang, Y. Ye, W. Tress, C. Yi, *Sci. Adv.* **2023**, *8*, 7422.
[16] N. Li, X. Niu, L. Li, H. Wang, Z. Huang, Y. Zhang, Y. Chen, X. Zhang, C. Zhu, H. Zai, Y. Bai, S. Ma, H. Liu, X. Liu, Z. Guo, G. Liu, R. Fan, H. Chen, J. Wang, Y. Lun, X. Wang, J. Hong, H. Xie, D. S. Jakob, X. G. Xu, Q. Chen, H. Zhou, *Science* **2021**, *373*, 561.
[17] F. Ye, T. Tian, J. Su, R. Jiang, J. Li, C. Jin, J. Tong, S. Bai, F. Huang, P. Müller-Buschbaum, Y. B. Cheng, T. Bu, *Adv. Energy Mater.* **2023**, *14*, 2302775.
[18] J. Peng, D. Walter, Y. Ren, M. Tebyetekerwa, Y. Wu, T. Duong, Q. Lin, J. Li, T. Lu, M. A. Mahmud, O. L. C. Lem, S. Zhao, W. Liu, Y. Liu, H. Shen, L. Li, F. Kremer, H. T. Nguyen, D. Y. Choi, K. J. Weber, K. R. Catchpole, T. P. White, *Science* **2021**, *371*, 390.
[19] C. Luo, G. Zheng, F. Gao, X. Wang, C. Zhan, X. Gao, Q. Zhao, *Nat. Photonics* **2023**, *17*, 856.
[20] T. Li, K. Mao, H. Meng, Z. Zhu, W. Peng, S. Yuan, J. Xu, X. Feng, Z. Xu, J. Xu, *Adv. Mater.* **2023**, *35*, 2211959.
[21] M. Kim, J. Jeong, H. Lu, T. K. Lee, F. T. Eickemeyer, Y. Liu, I. W. Choi, S. J. Choi, Y. Jo, H. B. Kim, S. I. Mo, Y. K. Kim, H. Lee, N. G. An, S. Cho, W. R. Tress, S. M. Zakeeruddin, A. Hagfeldt, J. Y. Kim, M. Grätzel, D. S. Kim, *Science* **2022**, *375*, 302.
[22] S. M. Park, M. Wei, N. Lempesis, W. Yu, T. Hossain, L. Agosta, V. Carnevali, H. R. Atapattu, P. Serles, F. T. Eickemeyer, H. Shin, M. Vafaie, D. Choi, K. Darabi, E. D. Jung, Y. Yang, D. B. Kim, S. M. Zakeeruddin, B. Chen, A. Amassian, T. Filleter, M. G. Kanatzidis, K. R. Graham, L. Xiao, U. Rothlisberger, M. Grätzel, E. H. Sargent, *Nature* **2023**, *624*, 289.
[23] S. Zhong, W. Wang, M. Tan, Y. Zhuang, W. Shen, *Adv. Sci.* **2017**, *4*, 1700200.
[24] M. De Bastiani, R. Jalmood, J. Liu, C. Ossig, A. Vlk, K. Vegso, M. Babics, F. H. Isikgor, A. S. Selvin, R. Azmi, E. Ugur, S. Banerjee, A. J. Mirabelli, E. Aydin, T. G. Allen, A. Ur Rehman, E. Van Kerschaver, P. Siffalovic, M. E. Stuckelberger, M. Ledinsky, S. De Wolf, *Adv. Funct. Mater.* **2023**, *33*, 2205557.
[25] H. Huang, P. Cui, Y. Chen, L. Yan, X. Yue, S. Qu, X. Wang, S. Du, B. Liu, Q. Zhang, Z. Lan, Y. Yang, J. Ji, X. Zhao, Y. Li, X. Wang, X. Ding, M. Li, *Joule* **2022**, *6*, 2186.
[26] T. Zhang, Q. He, J. Yu, A. Chen, Z. Zhang, J. Pan, *Nano Energy* **2022**, *104*, 107918.
[27] L. Lin, T. W. Jones, T. C. J. Yang, N. W. Duffy, J. Li, L. Zhao, B. Chi, X. Wang, G. J. Wilson, *Adv. Funct. Mater.* **2021**, *31*, 2008300.
[28] Q. Gao, S. Yang, L. Lei, S. Zhang, Q. Cao, J. Xie, J. Li, Y. Liu, *Chem. Lett.* **2015**, *44*, 624.

[29] H. Yang, R. Li, S. Gong, H. Wang, S. M. H. Qaid, Q. Zhou, W. Cai, X. Chen, J. Chen, Z. Zang, *Nano Lett.* **2023**, *23*, 8610.
[30] S. Kim, Y. J. Yun, T. Kim, C. Lee, Y. Ko, Y. Jun, *Chem. Mater.* **2021**, *33*, 8194.
[31] Z. Wu, J. Su, N. Chai, S. Cheng, X. Wang, Z. Zhang, X. Liu, H. Zhong, J. Yang, Z. Wang, J. Liu, X. Li, H. Lin, *Adv. Sci.* **2023**, *10*, 2300010.
[32] J. J. Yoo, G. Seo, M. R. Chua, T. G. Park, Y. Lu, F. Rotermund, Y. K. Kim, C. S. Moon, N. J. Jeon, J. P. Correa-Baena, V. Bulović, S. S. Shin, M. G. Bawendi, J. Seo, *Nature* **2021**, *590*, 587.
[33] X. Zhu, M. Du, J. Feng, H. Wang, Z. Xu, L. Wang, S. Zuo, C. Wang, Z. Wang, C. Zhang, X. Ren, S. Priya, D. Yang, S. Liu, *Angew. Chem., Int. Ed.* **2021**, *60*, 4238.
[34] J. Wu, J. Shi, Y. Li, H. Li, H. Wu, Y. Luo, D. Li, Q. Meng, *Adv. Energy Mater.* **2019**, *9*, 1901352.
[35] C. Chen, X. Wang, Z. Li, X. Du, Z. Shao, X. Sun, D. Liu, C. Gao, L. Hao, Q. Zhao, B. Zhang, G. Cui, S. Pang, *Angew. Chem., Int. Ed.* **2022**, *61*, e202113932.
[36] Y. Ko, T. Kim, C. Lee, C. Lee, Y. J. Yun, Y. Jun, *Energy Environ. Mater.* **2023**, *6*, e12347.
[37] Q. Tian, J. Yan, L. Yang, J. Chen, *Electrochim. Acta* **2018**, *282*, 38.
[38] Z. Hu, Z. Chen, Q. Liu, W. Zhao, Y. Xu, H. B. Wu, *iScience* **2023**, *26*, 106642.
[39] A. Mayabadi, A. Pawbake, S. Rondiya, A. Rokade, R. Waykar, R. Kulkarni, A. Jadhavar, M. Kamble, B. Gabhale, V. Waman, V. Sathe, H. Pathan, S. Jadkar, *Thin Solid Films* **2015**, *589*, 493.
[40] C. Li, H. Xu, C. Zhi, Z. Wan, Z. Li, *Chin. Phys. B* **2022**, *31*, 118802.
[41] J. Byeon, J. Kim, J. Y. Kim, G. Lee, K. Bang, N. Ahn, M. Choi, *ACS Energy Lett.* **2020**, *5*, 2580.
[42] N. Li, J. Yan, Y. Ai, E. Jiang, L. Lin, C. Shou, B. Yan, J. Sheng, J. Ye, *Sci. China Mater.* **2020**, *63*, 207.
[43] S. Song, G. Kang, L. Pyeon, C. Lim, G. Y. Lee, T. Park, J. Choi, *ACS Energy Lett.* **2017**, *2*, 2667.
[44] W. Tress, M. Yavari, K. Domanski, P. Yadav, B. Niesen, J. P. Correa Baena, A. Hagfeldt, M. Graetzel, *Energy Environ. Sci.* **2018**, *11*, 151.
[45] Z. Liu, K. Deng, J. Hu, L. Li, *Angew. Chem., Int. Ed.* **2019**, *58*, 11497.
[46] D. Zhao, C. Zhang, M. Zhao, J. Ren, Z. Dai, Y. Wu, Q. Sun, Y. Cui, Y. Hao, *J. Mater. Chem. C* **2022**, *10*, 7641.
[47] X. Yue, B. Fan, X. Zhao, Y. Yang, S. Qu, Q. Zhang, X. Sun, P. Cui, J. Ma, M. Li, *Sustain. Energy Fuels* **2023**, *7*, 727.
[48] C. H. Li, Z. Huang, J. Lin, T. Hou, Y. Zi, J. Li, *ACS Appl. Mater. Interfaces* **2023**, *15*, 35459.
[49] Y. Su, J. Shang, X. Liu, J. Li, Q. Pan, Y. Tang, *Angew. Chem., Int. Ed.* **2024**, e202403775.
[50] Q. Wali, M. Aamir, A. Ullah, F. J. Iftikhar, M. E. Khan, J. Akhtar, S. Yang, *Chem. Rec.* **2022**, *22*, e202100150.
[51] S. Fu, H. Wu, W. He, Q. Li, C. Shan, J. Wang, Y. Du, S. Du, Z. Huang, C. Hu, *Adv. Mater.* **2023**, *35*, 2302954.
[52] J. Ji, X. Liu, H. Jiang, M. Duan, B. Liu, H. Huang, D. Wei, Y. Li, M. Li, *iScience* **2020**, *23*, 101013.